Entanglement detection in a coupled atom-field system via quantum Fisher information

Safoura Sadat Mirkhalaf* and Augusto Smerzi
QSTAR, INO-CNR and LENS, Largo Enrico Fermi 2, 50125 Firenze, Italy
(Received 15 June 2016; published 2 February 2017)

We consider a system of finite number of particles collectively interacting with a single-mode coherent field inside a cavity. Depending on the strength of the initial field compared to the number of atoms, we consider three regimes of weak-, intermediate-, and strong-field interaction. The dynamics of multiparticle entanglement detected by quantum Fisher information and spin squeezing are studied in each regime. It is seen that in the weak-field regime, spin squeezing and quantum Fisher information coincide. However, by increasing the initial field population toward the strong-field regime, quantum Fisher information is more effective in detecting entanglement compared to spin squeezing. In addition, in the two-atom system, we also study concurrence. In this case, the quantum Fisher information as a function of time is in good agreement with concurrence in predicting entanglement peaks.

DOI: 10.1103/PhysRevA.95.022302

I. INTRODUCTION

The Dicke model [1], first discussed in 1954 by Dicke, consists of N two-level atoms which are coherently coupled to a single mode of radiation field. It was proved that the *collective* emission rate of N atoms in the same environment boosts by the factor N^2 (super-radiance) and not N as expected. The Dicke Hamiltonian is not generally integrable. Nevertheless, it is possible to use some approximations to simplify the model. In 1968, Tavis and Cummings solved the problem under the rotating-wave approximation (RWA) [2], which is valid for the weak atom-field coupling in the near-resonant situation.

In recent years, the Dicke model has experienced a renaissance of interest. The model has been realized in systems of a Bose-Einstein condensate coupled to a high-finesse cavity [3,4] as well as atoms in a cavity QED setup [5], and its phase transition [6,7] has been observed [3]. On the other hand, the Dicke model has been employed to study [8–10] and create [11,12] multiparticle entanglement. Being composed of atoms coherently coupled to the field, the system basically paves the way for exploring the different kinds of entanglement, e.g., atom-atom or/and atom-field entanglement. In this regard, multiparticle entangled states are not only interesting from a fundamental point of view, but also have practical applications in quantum information [13] and quantum metrology [14]. Particularly in the case of quantum metrology, it has been proved that exploiting the multiparticle entangled resources improves measurement precision beyond the "standard quantum limit." The essence of multiparticle entanglement in the Dicke model refers to the fact that the common field mode acts as a *virtual data bus* which mediates the interaction between the atoms at arbitrary positions.

All in all, despite the importance of entanglement, a global—necessary and sufficient—criterion for multiparticle entanglement does not exist. For the simplest case of a pair of particles, the concurrence $\mathcal{C}$ [15]—which is closely related to the entanglement of formation—has been widely used for quantifying the entanglement. However, when it comes to more than two particles, different measures have been used for different purposes. Thus, the choice of entanglement criterion itself is an issue depending on the application we want to harness the entanglement for. Specifically, in an ensemble of N particles, the spectroscopic spin squeezing [16] has been extensively used [17–20] as a criterion for detecting entanglement [21]. Nevertheless, spin-squeezed states are a small family of the whole multiparticle entangled states. In other words, while the all spin-squeezed states are entangled, the opposite statement is not necessarily true. For example, the important family of GHZ entangled states are not detectable using spin squeezing.

On the other hand, it has been proved [22] that quantum Fisher information (QFI) gives a sufficient condition for detecting entanglement in a multiparticle system. Being linked to phase estimation theory, QFI is also a sufficient and necessary criterion of metrological *useful entanglement* [23], which is desirable in atomic clocks [24] as well as quantum sensors [25]. In general, quantum Fisher information witnesses a larger family of entangled states than spin squeezing, including NOON or GHZ [26]. Experimentally, the entangled twin Fock [27] and non-Gaussian [28,29] spin states have been detected by measuring Fisher information.

In the following, we will use the quantum Fisher information to study the dynamics of entanglement among the finite number of particles interacting with a single coherent mode of the field. In a broad range of initial coherent fields, we detect multiparticle entanglement. For small atomic ensembles interacting with a strong coherent field, an oscillating entanglement signature is observed. In Sec. II, we introduce the physical model considering RWA. Afterward, in Sec. III, we briefly present the (multiparticle) entanglement witnesses that we use later, which are the quantum Fisher information flag, spin squeezing, and concurrence. In this work, our focus is on the quantum Fisher information flag, while we compare it with the other two measures frequently. In Sec. IV, we study the entanglement temporal behavior. Depending on the initial average photonic population $\bar{n}$ and number of atoms N, we consider three regimes of interaction, i.e., (a) *weak-field* ($\bar{n} \ll N$), (b) *intermediate-field* ($\bar{n} \sim N$), and (c) *strong-field* ($\bar{n} \gg N$) regimes, and investigate the dynamics of the QFI flag of the atomic subsystem. In the two extreme limits of

*Corresponding author: paperscontactmail@gmail.com

weak- and strong-field regimes, the analytical approximate outputs are discussed. The analysis and discussion of the results are presented in Sec. V, and in Sec. VI we give the conclusion.

II. THE MODEL AND ITS SOLUTIONS

We consider the resonant interaction between N two-level atoms with ground (excited) energy state $|g\rangle$ ($|e\rangle$) and the single mode of radiation field of frequency ω inside the cavity. The dipole and RWA approximations are imposed and we neglect the losses from both cavity and atoms. The interaction Hamiltonian of the system is given by ($\hbar = 1$)

$$H_{\rm int} = g(aS_+ + a^\dagger S_-). \tag{1}$$

Here, g is the atom-field interaction strength and a ($a^\dagger$) is the annihilation (creation) operator of the field. Moreover, $S_\pm = S_x \pm i S_y$ are defined in terms of the standard Pauli matrices via $S_\alpha = \frac{1}{2}\sum_{i=1}^{N}\sigma_\alpha^{(i)}$ ($\alpha \in \{x,y,z\}$). The constants of motion are $a^\dagger a + S_z$ and $S^2 = S_z^2 + (S_+S_- + S_-S_+)/2$. In the case of symmetry under any permutation of the particles, the atomic states are conveniently described by Dicke states, $|N/2,M\rangle$, which are the simultaneous eigenvectors of S^2 and S_z with $-N/2 \leqslant M \leqslant N/2$.

During this work, we assume that all of the atoms are initially in the ground state, $|N/2,-N/2\rangle$, and the initial field is a coherent state,

$$|\alpha\rangle = e^{-|\alpha|^2/2}\sum_{n=0}^{\infty}\frac{\alpha^n}{\sqrt{n!}}|n\rangle \equiv \sum_{n=0}^{\infty}c_n|n\rangle, \tag{2}$$

with $|n\rangle$ referring to Fock states of the field with probability amplitude c_n. For simplicity, we consider real values of α. Therefore, the initial state of the system is

$$|\psi(0)\rangle = \sum_{n=0}^{\infty}c_n|N/2,-N/2\rangle \otimes |n\rangle. \tag{3}$$

The Hilbert space of the joint atom-field system is given by the tensor product $\mathcal{H} = \mathcal{H}_a \otimes \mathcal{H}_f$, where $\mathcal{H}_a$ and $\mathcal{H}_f$ denote the Hilbert space of atoms and electromagnetic field, respectively. In general, the Hilbert space of the atomic state has the dimension of $N+1$, while the latter has infinite dimensions. In order to apply the numerical calculations, we have imposed a cutoff on the number of bosons in the field such that there is no modification in the final results by its change.

In the interaction picture, the wave function of the system is expressed as

$$|\psi(t)\rangle = \sum_{M=-N/2}^{N/2}\sum_{n=0}^{\infty}C_{M,n}(t)e^{-i\omega(M+n)t}|N/2,M\rangle \otimes |n\rangle, \tag{4}$$

where $C_{M,n}$ is the probability amplitude of being the system in $|N/2,M\rangle$ and $|n\rangle$ atomic and field states, respectively. By applying the Hamiltonian (1) over (4), the equation of motion gives

$$\dot{C}_{M,n} = -ig\left\{\sqrt{\left(\frac{N}{2}+M\right)\left(\frac{N}{2}-M+1\right)}(n+1)C_{M-1,n+1} + \sqrt{\left(\frac{N}{2}-M\right)\left(\frac{N}{2}+M+1\right)}nC_{M+1,n-1}\right\}, \tag{5}$$

where the initial condition is $C_{M,n}(0) = c_n\delta_{M,-N/2}$. Generally, this equation represents the coupled set of equations from $M = -N/2$ to $N/2$. Nevertheless, in practice, depending on the initial photonic population, the set of equations couple up to $-N/2 + n_{\rm max}$, where $n_{\rm max}$ is the smallest populated Fock state of the field with nonzero amplitude c_n [30].

III. MULTIPARTICLE ENTANGLEMENT WITNESSES

In order to detect multiparticle entanglement in a physical system, many different witnesses (detectors) have been presented [21,22,31–33]. In the following, we are mainly interested in quantum Fisher information as well as spin squeezing, which are both linked to quantum metrology applications.

Let us consider an ensemble of spin-half particles in a mixed state. Specifically, for the coupled atom-field system introduced in Sec. II, this mixed state would be the reduced atomic density matrix after tracing out the field degrees of freedom, $\rho_a = {\rm tr}_f|\psi\rangle\langle\psi| = \sum_i p_i|\phi_i\rangle\langle\phi_i|$. Here, p_i and $|\phi_i\rangle$ represent the eigenvalues and eigenstates of the atomic density matrix ρ_a. The quantum Fisher information for the multispin system is given by [22]

$$F(\rho_a, S_{\vec{n}}) = 2\sum_{i\neq j}\frac{(p_i-p_j)^2}{p_i+p_j}|\langle\phi_i|S_{\vec{n}}|\phi_j\rangle|^2, \tag{6}$$

with $S_{\vec{n}}$ being the collective spin operator along direction $\vec{n}$, i.e., $S_{\vec{n}} = \vec{S}\cdot\vec{n}$. It has been proved that the quantity

$$\chi^2 \equiv \frac{N}{\max\{F(\rho_a, S_{\vec{n}})\}} \tag{7}$$

implies multiparticle entanglement when $\chi^2 < 1$ [22]. The maximization in the denominator of Eq. (7) is taken over all possible directions of $\vec{n}$. Since χ^2 detects (flags) entanglement, we call it the quantum Fisher information flag [34] in the following. The upper bound of F for an N-spin system is N^2, which is saturated for maximally entangled states [26]. This corresponds to the ultimate QFI flag of $1/N$. On the other hand, the quantum Fisher information F for the spin coherent states [35] is N, which gives the shot-noise limit, $\chi^2 = 1$ [22]. The inequality $\chi^2 < 1$ is a sufficient condition for multiparticle entanglement and a necessary and sufficient condition for detecting the useful entanglement [23]. The term useful refers to the family of entangled states which enhances the interferometry precision beyond the classical limit when used as the input resource.

On the other hand, the relation between spectroscopic spin squeezing [16],

$$\xi^2 = \frac{N\min\{\Delta S_\perp^2\}}{|\langle S\rangle|^2}, \tag{8}$$

and multiparticle entanglement has been established by $\xi^2 < 1$ [21]. In Eq. (8), $|\langle S\rangle| = \sqrt{\langle S_x\rangle^2 + \langle S_y\rangle^2 + \langle S_z\rangle^2}$ is the mean spin length, while $S_\perp$ represents the spin directions normal to the mean spin. The minimization in the nominator of Eq. (8) should be taken over all normal directions. It is proved [22] that the quantum Fisher information as an entanglement criterion is stronger than spin squeezing $\chi^2 \leqslant \xi^2$, while it is more difficult to measure in practice.

Moreover, Wootters concurrence is used as a quantifier of pairwise entanglement [15],

$$\mathcal{C} = \max\{0, \lambda_1 - \lambda_2 - \lambda_3 - \lambda_4\}, \tag{9}$$

where the quantities λ_i are the square roots of the eigenvalues in the matrix product $\varrho_{12} = \rho_{12}(\sigma_{1y} \otimes \sigma_{2y})\rho_{12}^*(\sigma_{1y} \otimes \sigma_{2y})$ in descending order. Here, ρ_{12} denotes the two-particle density matrix. The value of $\mathcal{C}$ varies between 0 and 1, indicating the separable and maximally entangled states, respectively. In this work, we also use the concurrence as an entanglement measure for two-atom systems.

IV. ENTANGLEMENT DETECTION

In this section, we study the dynamics of the QFI flag in comparison with spin squeezing in order to detect multiparticle entanglement in the three regimes of interaction.

A. Weak-field limit

When $\bar{n}$ is much less than the number of atoms N, we are in the weak-field regime. In order to get the analytical results, let us take $\bar{n} = |\alpha|^2 \ll 1$. In this case, one can expand the field amplitudes c_n in (2) up to terms of α^2 and dismiss the upper orders approximately. By solving the equation of motion (5), the lowest-order nonvanishing coherent amplitudes are [30]

$$\begin{aligned}
C_{-N/2,0}(t) &= 1 - \alpha^2/2,\\
C_{-N/2,1}(t) &= \alpha\cos(\sqrt{N}gt),\\
C_{-N/2,2}(t) &= \frac{\alpha^2\sqrt{2}}{4N-2}[N - 1 + N\cos(\sqrt{4N-2}gt)],\\
C_{-N/2+1,0}(t) &= -i\alpha\sin(\sqrt{N}gt),\\
C_{-N/2+1,1}(t) &= -\frac{i\alpha^2\sqrt{N}}{\sqrt{4N-2}}\sin(\sqrt{4N-2}gt),\\
C_{-N/2+2,0}(t) &= -\frac{\alpha^2\sqrt{2N(N-1)}}{4N-2}[1 - \cos(\sqrt{4N-2}gt)],
\end{aligned} \tag{10}$$

which lead to the following average spin components:

$$\begin{aligned}
\langle S_x(t)\rangle &= 0,\\
\langle S_y(t)\rangle &= \sqrt{N}\alpha\sin(\sqrt{N}gt),\\
\langle S_z(t)\rangle &= -\frac{N}{2} + \alpha^2\sin^2(\sqrt{N}gt).
\end{aligned} \tag{11}$$

One observes that the mean spin direction is in a plane normal to the x direction (yz plane) with $|\langle S\rangle| \approx N/2$. Moreover, Eqs. (10) give $1 - \mathrm{tr}(\rho_a^2) \approx 0$; i.e., the atomic state is pure and thus (6) simplifies to $F = 4\Delta S_{\bar{n}}^2$ [22]. Hence, the quantum Fisher information flag (7) may be written as

$$\chi^2 = \frac{N}{4\max\{(\Delta S_{\bar{n}})^2\}}. \tag{12}$$

Now, let us take an axes yz in the plane perpendicular to the mean spin direction and x. By optimizing ΔS_n^2 in (12), we get $\Delta S_{\bar{n}}^2 \leqslant \max\{\Delta S_x^2, \Delta S_{yz}^2\}$ [36]. Correspondingly, if $S_\perp = \cos\theta S_x + \sin\theta S_{yz}$ in (8), one finds $\Delta S_\perp^2 \geqslant \min\{\Delta S_x^2, \Delta S_{yz}^2\}$ [37]. It means that the optimal spin variance is either along x or yz. Thus,

$$\chi^2 = \frac{N}{4\max\{\Delta S_x^2, \Delta S_{yz}^2\}}, \tag{13}$$

and

$$\xi^2 = \frac{4\min\left\{\Delta S_x^2, \Delta S_{yz}^2\right\}}{N}, \tag{14}$$

with the following spin fluctuations in normal directions:

$$\begin{aligned}
\Delta S_x^2(t) &\approx N/4 + N\bar{n}\left\{\frac{N-1}{N}\sin^2(\sqrt{N}gt)\right.\\
&\quad\left.-\frac{2(N-1)}{2N-1}\sin^2[\sqrt{(2N-1)/2}gt]\right\}\Big/2,\\
\Delta S_{yz}^2(t) &\approx N/4 - N\bar{n}\left\{\frac{N-1}{N}\sin^2(\sqrt{N}gt)\right.\\
&\quad\left.-\frac{2(N-1)}{2N-1}\sin^2[\sqrt{(2N-1)/2}gt]\right\}\Big/2.
\end{aligned} \tag{15}$$

Specifically, from Eqs. (15), we get

$$\Delta S_x^2\Delta S_{yz}^2 \approx \frac{N^2}{16} = \frac{|\langle S\rangle|^2}{4}. \tag{16}$$

This means that if the maximum of normal spin is along S_x, its minimum occurs along S_{yz}, and vice versa. Making use of Eqs. (13), (14), and (16), we get $\chi^2 = \xi^2$. This equality is a reduced form of $\chi^2 \leqslant \xi^2$, which is valid for minimum uncertainty (Gaussian) spin states.

From spin variances of (15) and (13), we get the slow and fast periods of χ^2 equal to $4\pi\sqrt{N}$ and $\pi/2\sqrt{N}$, respectively (unit of g). The first quantity is known to be the revival time of the Tavis-Cummings model in a weak-field regime extracted by perturbation theory [38,39]. Moreover, we can find that the minimum of χ^2—being of the order of $\sim 1 - 2\bar{n}$—occurs at $2\pi\sqrt{N}$. Thus, by increasing the number of particles, maximum entanglement take place at longer times.

Figure 1 gives the time evolution of the optimal quantum Fisher information flag for $N = 2$ and $\bar{n} = 0.01$ by exact numerical simulations. Furthermore, the analytical results along x and yz are given using Eqs. (13) and (15). The envelope of χ^2 has the period of $4\pi\sqrt{2} = 17.78$. In order to exactly calculate χ^2, we have numerically solved the equation of motion (5) for the joint atom-field system. Thereafter, the reduced atomic density matrix has been used in Eqs. (6) and (7).

To investigate the effect of increasing N on entanglement, in Fig. 2, we have plotted the minimum of the envelope of χ^2 versus N for $\bar{n} = 0.1$ derived with numerical simulations. One observes that by increasing the number of particles, $\chi^2_{\min}$ decreases. However, as we see, the amount of entanglement is

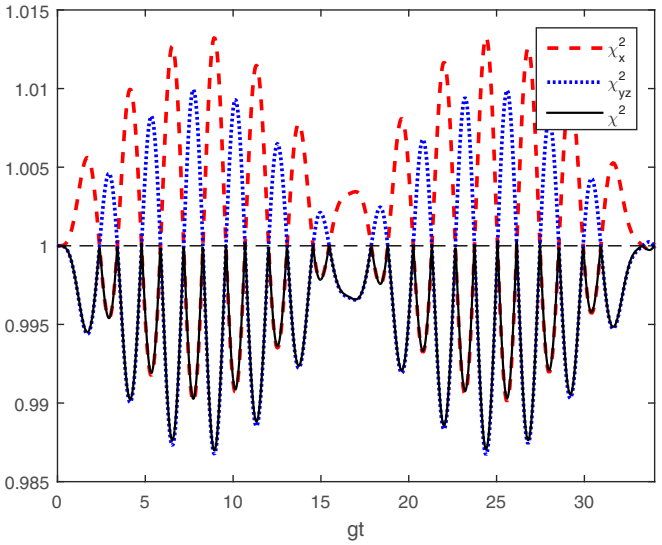

FIG. 1. Quantum Fisher information flag along χ_x^2 (dashed red), χ_{yz}^2 (dotted blue), and optimal direction χ^2 (solid black) as a function of gt for $N = 2$ and $\bar{n} = 0.01$.

not very large. This is in agreement with the spin-squeezing results given in Ref. [30].

For a system composed of a pair of particles, it is interesting to compare χ^2 with the pairwise entanglement measured by concurrence (9). In Fig. 3, we have plotted the quantum Fisher information flag χ^2, concurrence $\mathcal{C}$, and linear entropy $1 - \mathrm{tr}(\rho_a^2)$ for $\bar{n} = 0.1$. We see a good agreement in the peaks of entanglement measures. Moreover, $1 - \mathrm{tr}(\rho_a^2) \approx 0$ indicates that the collective spin state remains almost pure during interaction. The linear entropy has been used as a measure of bimodal entanglement in atom-field interaction systems [8,41].

We would like to add that for a system having a number of atoms much larger than unity and much larger than the average number of photons in the field, it is possible to use perturbation theory along with the Holstein-Primakoff approximations to generalize the analytical results in the wider range of $\bar{n} \ll N$. The same procedure has been used to get the spin [30] and

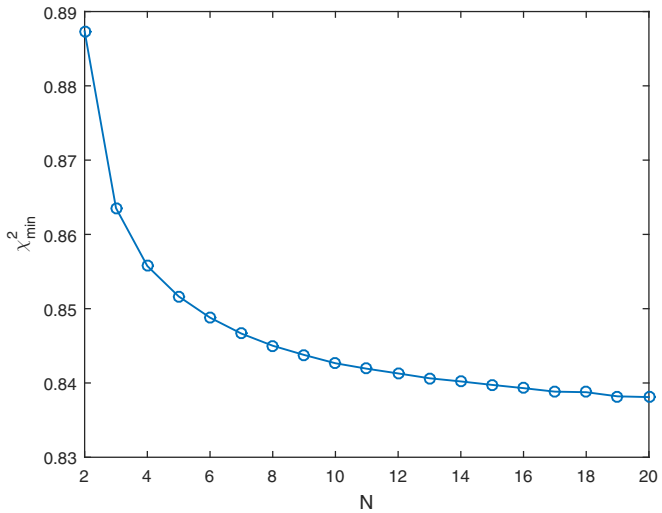

FIG. 2. The minimum values of χ^2 as a function of N for $\bar{n} = 0.1$.

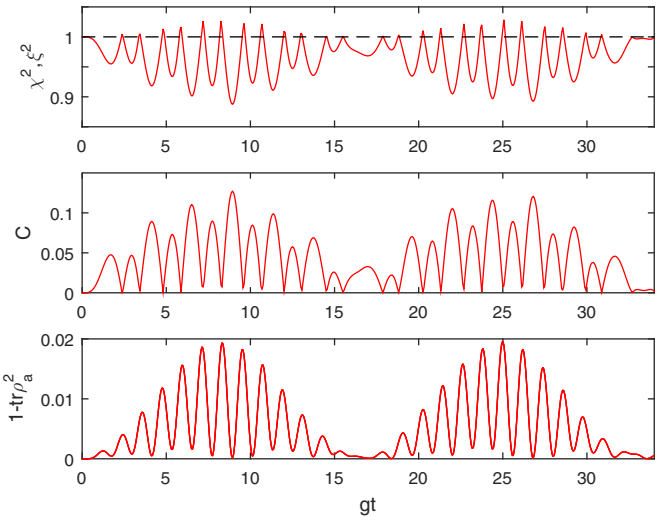

FIG. 3. Time evolution of $\chi^2 (= \xi^2)$ (upper panel), concurrence $\mathcal{C}$ (middle panel), and $1 - \mathrm{tr}\rho_a^2$ (lower panel) for $N = 2$ and $\bar{n} = 0.1$.

field [42] squeezing. In our work, the analytical results are sufficient as we consider small ensembles of particles with weak-field regimes which practically do not exceed much in the $\bar{n} > 1$ range.

All in all, in the weak-field regime composed of small ensembles, the entanglement amount is moderate. Thus, in the next sections, we discuss the effect of stronger initial coherent fields on entanglement witnesses.

B. Intermediate-field limit

In the intermediate-field limit, we consider the initial photonic population of the order of number of atoms $\bar{n} \sim N$. In this regime, one has to consider coefficients with upper orders of α in (2) and we have used the numerical simulations to solve the equation of motion (5). Figure 4 gives the quantum Fisher information flag χ^2, spin squeezing ξ^2, and concurrence $\mathcal{C}$

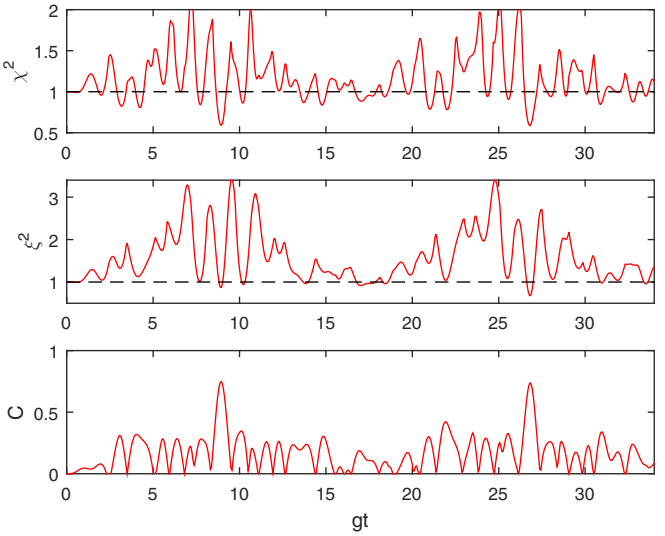

FIG. 4. Time evolutions of χ^2 (upper panel), ξ^2 (middle panel), and $\mathcal{C}$ (lower panel) for $N = 2$ and $\bar{n} = 1$.

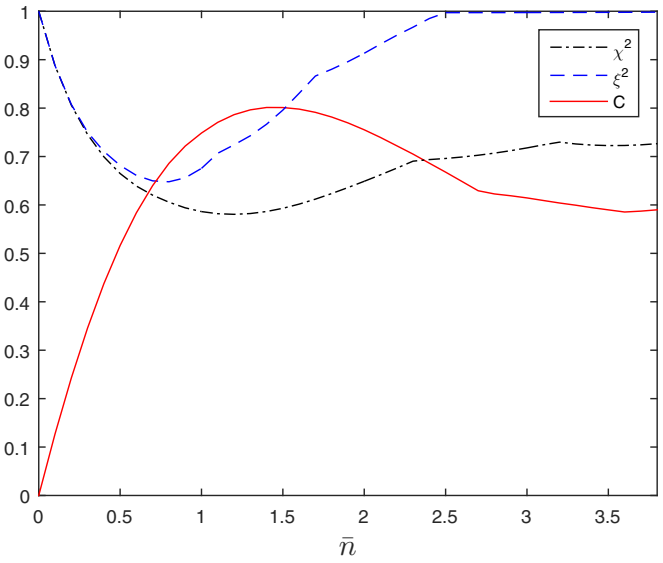

FIG. 5. The minimum values of χ^2 (dash-dotted black), minimums of ξ^2 (dashed blue), and maximums of $\mathcal{C}$ (solid red) as a function of $\bar{n}$ for $N = 2$ ($gt_{\rm cutoff} = 200$).

as a function of gt for $N = 2$ and $\bar{n} = 1$. At first glance, we observe that by increasing $\bar{n}$, the entanglement measures lose their regular behaviors of the weak-field regime. Moreover, the χ^2 and ξ^2 do not coincide, while there is relatively more agreement in entanglement peaks between χ^2 and $\mathcal{C}$. We have to keep in mind that the QFI and concurrence do not necessarily coincide, in general. This is due to the fact that the kind of entanglement detected by QFI has the feature of being useful for interferometric proposes. This condition is not always met when we utilize concurrence as an entanglement measure.

To observe the effect of increasing the initial coherent field population on entanglement, in Fig. 5, the minimums of quantum Fisher information flag χ^2, minimums of spin squeezing ξ^2, and maximums of concurrence $\mathcal{C}$ versus $\bar{n}$ are given. To get to this plot, we have put a cutoff on time at $gt_{\rm cutoff} = 200$ and then, for every $\bar{n}$, we have extracted the optimal values of entanglement measures over the time span. Moreover, we have replaced any $\chi^2,\xi^2 > 1$ with unity because we are interested in the multiparticle entangled states (neither coherent nor unentangled states).

Figure 5 shows that when we go beyond the weak regime, the quantum Fisher information flag begins to detect more entanglement than spin squeezing ($\chi^2 < \xi^2$). As we see, by increasing the initial field population in the intermediate-field regime, both metrological measures decrease up to certain minimums for their respective values of $\bar{n}$. Nevertheless, after surpassing these peaks, there are different trends for χ^2 and ξ^2 with increasing $\bar{n}$. In this case, spin squeezing decreases and is almost diminished for $\bar{n} > 2.5$. On the other hand, the quantum Fisher information flag varies while it keeps $\chi^2 < 1$. This indicates the presence of multiparticle entanglement even if there are moderate coherent fields in the system. We can see the same qualitative behavior as the QFI flag for the concurrence in the same figure.

Furthermore, we have noticed that the minimums of the quantum Fisher information flag occur at longer time scales than the weak-field regime. For example, for $N = 2$ and $\bar{n} = 5$, we have found the optimal value of χ^2 at $gt_{\rm min} = 195.5$, which resides very close to the cutoff bound ($gt_{\rm cutoff} = 200$), while for the weak field of $\bar{n} = 0.1$, we get it at $gt_{\rm min} \approx 2\pi\sqrt{2} = 8.88$. The same behavior for spin squeezing has been reported [30].

We have derived similar plots for different numbers of particles within $2 \leqslant N \leqslant 20$ for χ^2 and ξ^2 versus $\bar{n}$ [43]. The typical behavior is that by increasing the initial field intensity, χ^2 and ξ^2 decrease up to their respective minimums. Afterward, while the spin squeezing decreases and approaches unity, quantum Fisher information makes some variations and show other local peaks; but it remains $\chi^2 < 1$. The point is that by passing the weak-field regime, the spin-squeezing and quantum Fisher information values begin to defer and we see $\chi^2 < \xi^2$. For instance, when $N = 10$ and 16, we have the optimal values of $\chi^2_{\rm min}/\xi^2_{\rm min} \approx 0.22/0.63$ and $0.17/0.61$ corresponding to the respective optimal $\bar{n}$'s in the intermediate regime.

Note that the values of spin squeezing and quantum Fisher information in Fig. 5 (and similar plots for $N > 2$) are obtained considering a chosen cutoff on time. Consequently, these values are not the most global optimized factors. Nevertheless, they give the general trend of entanglement. All in all, in the intermediate-field regime, there is not a regular behavior in the QFI flag (and, correspondingly, the entanglement dynamics) and the optimal values may occur in very long times. This is a flaw when it comes to measure the entanglement, in practice. In the next section, we study the entanglement dynamics when the atomic ensemble is interacting with strong coherent fields.

C. Strong-field limit

In the strong-field regime $\bar{n} \gg N$, we can get the approximate solutions for the dynamics of the system (and principally χ^2) taking advantage of factorization approximations, which is discussed as follows.

For large coherent photonic populations, the boson operators of the field are replaced with c-numbers, $a,a^\dagger \to \alpha \equiv \sqrt{\bar{n}}$, and the interaction Hamiltonian (1) reduces to the semiclassical form of $H_{cl} = 2g\sqrt{\bar{n}}S_x$. Correspondingly, the semiclassical states are defined as simultaneous eigenfunctions of H_{cl} and S_x such that $S_x|N/2,m_x\rangle_x = m_x|N/2,m_x\rangle_x$. If atoms initiate in a semiclassical state and the field in a strong coherent state, the factorization approximation implies that the wave function of the joint system can be approximately written as a factorized product of the atomic $|A_{mx}(t)\rangle$ and field parts $|\Phi_{mx}(t)\rangle$ such that $|\psi(t)\rangle \cong |A_{mx}(t)\rangle \otimes |\Phi_{mx}(t)\rangle$ [44,45]. The validity range of the approximation is for times which are short compared to $t \approx \bar{n}/g$ and accuracy of order $N/\sqrt{\bar{n}}$ [44,45]. The semiclassical states form a convenient (complete) basis to use in describing the state of the atomic ensemble. Therefore, any arbitrary initial state of the atom-field system (including 3) is given by

$$|\psi(0)\rangle = \sum_{mx=-N/2}^{N/2} d_{mx}|N/2,m_x\rangle_x \otimes |\alpha\rangle, \qquad (17)$$

where $|d_{mx}|^2$ is the probability of atoms being initially in the semiclassical state $|N/2,m_x\rangle_x$. Correspondingly, the atom-field state can be written as a superposition of factorized states

at any time t,

$$|\psi(t)\rangle = \sum_{mx=-N/2}^{N/2} d_{mx}|A_{mx}(t)\rangle \otimes |\Phi_{mx}(t)\rangle. \quad (18)$$

In order to get the analytical results for the quantum Fisher information flag χ^2, let us begin with $N = 2$ and discuss the larger ensembles in the following. For a two-atom system, three symmetric eigenstates of S_x are labelled by $m_x = -1,0,$ and 1. Thus, Eq. (18) gives the state of the system as $|\psi(t)\rangle = \sum_{mx=-1}^{1} d_{mx}|A_{mx}(t)\rangle \otimes |\Phi_{mx}(t)\rangle$. After tracing out the field degrees of freedom, the reduced two-atom density matrix is obtained as

$$\rho_a(t) = \sum_{mx,lx} d_{mx}d_{lx}^{*}|A_{mx}(t)\rangle\langle A_{lx}(t)|f_{ml}(gt,\bar{n}), \quad (19)$$

where $f_{ml}(gt,\bar{n}) = \sum_n \langle n|\Phi_{mx}(t)\rangle\langle\Phi_{lx}(t)|n\rangle$. As explained in Ref. [8], this function has memory only for $t \ll \sqrt{\bar{n}}/g$ and afterward shows a δ-function behavior. In fact, the presence of large-dimensional Hilbert space of the field resembles a reservoir for the atoms. In this case, the atomic states $|A_m(t)\rangle$ act effectively as a pointer basis for decoherence of the atomic density matrix. This Markoff approximation is valid for times of the order of $2\pi\sqrt{\bar{n}}/g$. Consequently, one gets the density matrix of atoms in the semiclassical basis as $\rho_a(t) \approx \sum_{mx} |d_{mx}|^2|A_{mx}(t)\rangle\langle A_{mx}(t)|$ [8]. For two atoms in the initial ground state $|gg\rangle$, we have $d_1 = d_{-1} = \frac{1}{2}$, $d_0 = \frac{1}{\sqrt{2}}$. As a result, the reduced atomic density matrix is obtained as

$$\rho_a(t) = \begin{pmatrix} \frac{3}{8} & -\frac{i}{4\sqrt{2}}\sin(t') & \frac{\cos(2t')}{8} - \frac{1}{4} \\ \frac{i}{4\sqrt{2}}\sin(t') & \frac{2}{8} & -\frac{i}{4\sqrt{2}}\sin(t') \\ \frac{\cos(2t')}{8} - \frac{1}{4} & \frac{i}{4\sqrt{2}}\sin(t') & \frac{3}{8} \end{pmatrix}, \quad (20)$$

with $t' = gt/\sqrt{\bar{n}}$. From the above equation, we get $\mathrm{tr}(\rho_a^2) < 1$. Therefore, the atomic state is mixed and we must use the general definition of F given in (6) [46]. In fact, in the weak-field limit, we used the reduced form of $F = 4\Delta S_n^2$, since the atomic state remains approximately pure during the time evolution. By diagonalization of the atomic density matrix (20) followed by using Eqs. (6) and (7), one gets the analytical expression for χ^2. We have not brought the final form of the quantum Fisher information flag due to the lengthiness. Instead, the ultimate analytical as well as exact numerical solutions of χ^2 as a function of gt are given in Fig. 6. Here, we have given the QFI flag along the optimal z direction where there is a reasonable agreement with the exact results in the validity region of the approximations. The violation of the results in the very short times and also $\pi\sqrt{\bar{n}}/g$ is due to breaking the Markoff approximations in this region [8]. All in all, the values in which $\chi^2 > 1$ are not interesting from an entanglement point of view.

In the two-atom system, the quantum Fisher information flag χ^2 shows a quasiregular behavior with the period of $\pi\sqrt{\bar{n}}/g$ and minimum values in every half period (see Fig. 6). The approximate minimums are derived equal to 2/3. In reality, after a number of periods, the quasiregular pattern of χ^2 is lost while entanglement eventually decays. The irregularities of χ^2 are related to the loss of regularities of atomic inversion.

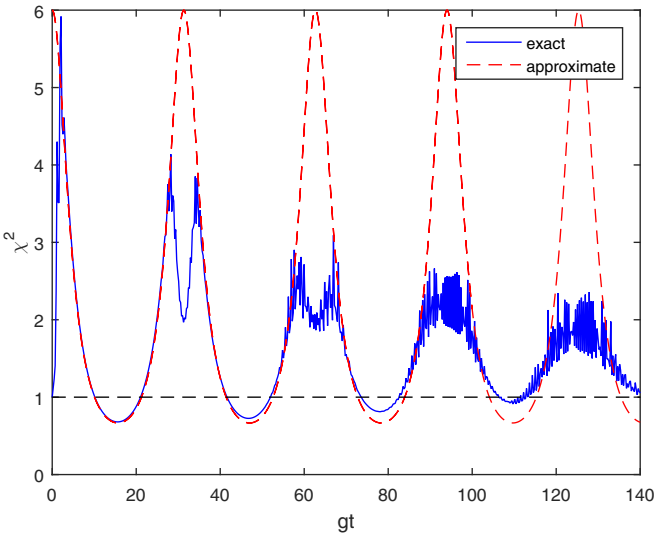

FIG. 6. Time evolution of χ^2 within exact (solid blue) and approximate (dashed red) approaches for $N = 2$ and $\bar{n} = 100$.

In fact, as time passes, the neighboring revivals begin to spread and finally overlap. Losing regularities with increasing time in the large coherent field limit has been observed for concurrence [8,47] and squeezing of the field [42].

In Fig. 7, we have given the temporal behavior of the χ^2 (upper panel) and $\mathcal{C}$ (middle panel) for $N = 2$ and $\bar{n} = 100$, which are consistent in predicting peaks of entanglement. For the two-qubit systems, concurrence is a sufficient and necessary witness of entanglement, while QFI detects the particular family of metrologically useful entangled states. Thus, these measures do not necessarily coincide all the time. The linear entropy $1 - \mathrm{tr}(\rho_a^2)$ in the lower part shows the mixed nature of the atomic state in this regime. Moreover, to investigate the effect of increasing $\bar{n}$ on entanglement measures, in Fig. 8, we have used the exact numerical results to plot the first minimum of χ^2 and first maximum of $\mathcal{C}$ as a function of $\bar{n}$. By increasing the coherent field strength, the

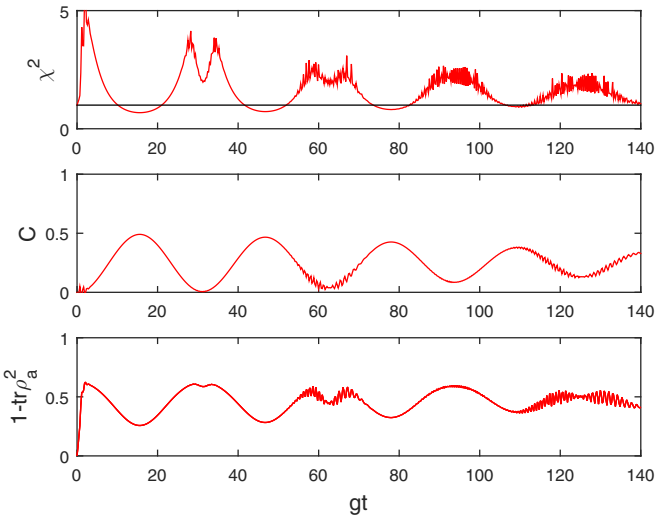

FIG. 7. χ^2 (upper panel), $\mathcal{C}$ (middle panel), and $1 - \mathrm{tr}\rho_a^2$ (lower panel) as a function of gt for $N = 2$ and $\bar{n} = 100$.

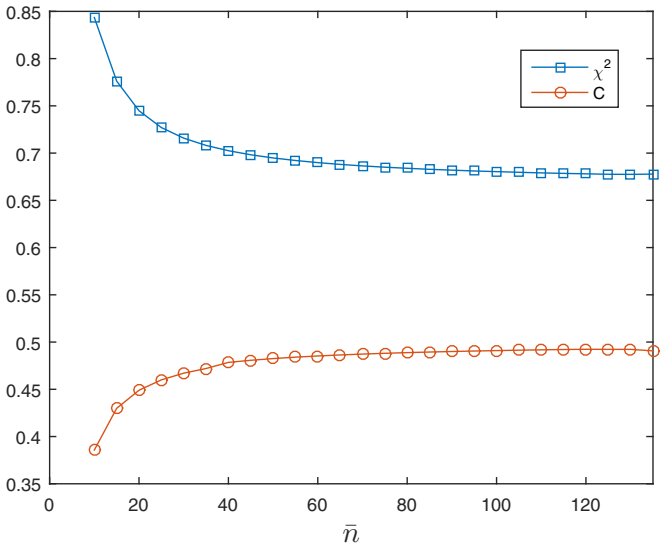

FIG. 8. The first minimum of χ^2 (squared blue) and the first maximum of $\mathcal{C}$ (circled red) vs $\bar{n}$ for $N = 2$.

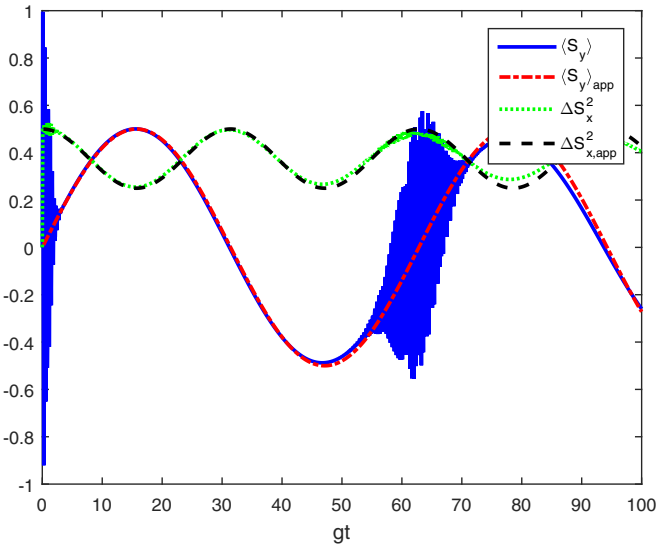

FIG. 9. Time evolutions of exact $\langle S_y\rangle$ (solid blue), approximate $\langle S_y\rangle_{\rm app}$ (dashed red), exact ΔS_x^2 (dotted green), and approximate $\Delta S_{x,\rm app}^2$ (dashed black) solutions with $N = 2$ and $\bar{n} = 100$.

minimum value of χ^2 decreases and eventually approaches to an asymptotic value in agreement with $\mathcal{C}$. The asymptotic limit of $2/3$ are the minimum values of χ^2, which is derived from factorization and Markoff approximations for strong enough fields.

On the other hand, it has already been discussed in Ref. [30] that the spin squeezing approaches unity and effectively vanishes moving toward strong-field limits. In this case, the Mollow transformations [48] has been employed to transform the interaction Hamiltonian to that of a classical field having amplitude α plus a fluctuating field. The decreasing of spin squeezing by increasing α has been attributed to decreasing the ratio of the fluctuations to the average field strength. It is possible to verify this for $N = 2$. Using the atomic density matrix (20), one gets the explicit expressions for the mean spin values,

$$\begin{aligned}\langle S_x(t)\rangle &= 0,\\ \langle S_y(t)\rangle &= \frac{\sin(gt/\sqrt{\bar{n}})}{2},\\ \langle S_z(t)\rangle &= 0,\end{aligned} \tag{21}$$

and the corresponding variances [49],

$$\begin{aligned}\Delta S_x^2 &= \frac{\cos(2gt/\sqrt{\bar{n}})}{8} + \frac{3}{8},\\ \Delta S_y^2 &= \frac{3}{4},\\ \Delta S_z^2 &= \frac{3}{4}\end{aligned} \tag{22}$$

(see Fig. 9). Equations (21) show that the mean spin direction is along y and always satisfies $0 \leqslant |\langle S\rangle|^2 \leqslant 1/4$. As a result, the normal spin fluctuations are located in the xz plane. Using optimal rotations in this plane, we get the minimum value of spin squeezing (8) along x, which fulfills $1/4 \leqslant \Delta S_x^2 \leqslant 1/2$ [50]. Consequently, the spin squeezing (8) gives $\xi^2 > 1$ (within the range of approximations).

Finally, let us consider the strong-field limit for $\bar{n} \gg N > 2$. By increasing both N and $\bar{n}$, the full numerical simulations get more cumbersome due to the significant size of the Hilbert space. Nevertheless, it is possible to derive the approximate solutions for the wave function of the system and principally get χ^2. Making use of Markoff and factorization approximations, we have extracted the dynamics of χ^2 as a function of gt. The interesting finding is that in small ensembles of particles, a quasiregular pattern of χ^2 and correspondingly entanglement dynamics regain. Our approximate solutions suggest that the minimums of χ^2—of the order of $\sim 2/(N+1)$—occur around odd multiples of $\pi\sqrt{\bar{n}}/N$. However, the structure of the oscillations of χ^2 becomes more complicated by increasing N. Figure 10 gives the temporal behavior of χ^2 for $N = 4$ and $\bar{n} = 100$, which declare the semiregular pattern of the

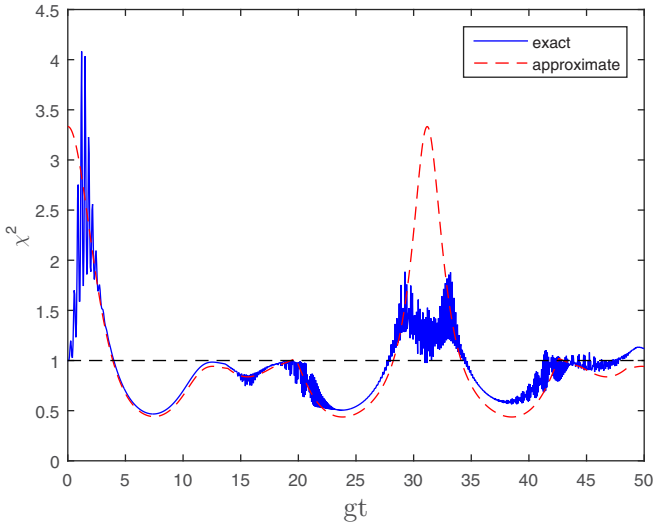

FIG. 10. Quantum Fisher information flag χ^2 vs time gt for $N = 4$ and $\bar{n} = 100$.

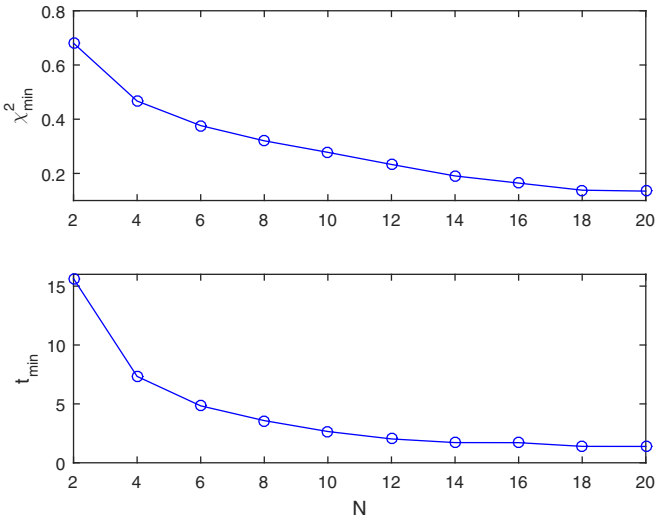

FIG. 11. The first minimum of quantum Fisher information flag $\chi^2_{\min}$ (upper panel) and its corresponding time $t_{\min}$ (lower panel) vs N for $\bar{n} = 100$.

entanglement. By increasing the ratio of $N/\sqrt{\bar{n}}$, the violation of the approximate results from exact ones increases due to decreasing the accuracy of factorization approximation.

In order to observe the effect of increasing N on entanglement, in Fig. 11, we have plotted the first minimums of χ^2 for different number of atoms (upper panel) when $\bar{n} = 100$. The amount of entanglement detected by χ^2 grows with increasing N with the factor around $\chi^2_{\min} \approx 1.1N^{-0.63}$ compared to N^{-1} which is the Heisenberg limit. In the lower panel of the same figure, we have given the time in which the first minimums occur, $t_{\min}$. We see that as opposed to the weak-field regime, with increasing the number of particles, $t_{\min}$ decreases. For the given data in Fig. 11, we have derived $t_{\min} = 33N^{-1.1} \cong O(\pi\sqrt{\bar{n}}/N)$.

It is worthwhile to mention that the regular and semiregular dynamics of the Tavis-Cummings model—in the weak- and strong-field regime—has been studied [38,39]; probably the most known effect is the collapse and revival of the population inversion of the atomic system. Moreover, the collapse and revival of entanglement for Schrödinger cat states in the strong-field regime has been studied [51,52].

By approaching very strong fields, the interaction Hamiltonian (1) reduces to the semiclassical Hamiltonian which is proportional to S_x and not capable of creating multiparticle entanglement. We can understand this by considering the fact that with increasing the initial photonic population, the minimum value of χ^2 occurs in longer time scales (with a factor $\sim\sqrt{\bar{n}}$). Thus, for $\bar{n} \to \infty$, the first minimum appears in a very long time, i.e., no entanglement appears.

V. DISCUSSION AND ANALYSIS

In this section, we briefly summarize all of the findings of the three regimes of interaction.

In the weak-field regime, the dynamics of the system is known to be regular making use of perturbation theory [38,39]. Here, we have derived a regular function of χ^2 versus time which coincides with spin squeezing ξ^2 because of the Gaussian nature of atomic spin states. The minimum amount of entanglement increases with increasing the amplitude of the field $\propto 1 - 2\bar{n}$, while it is moderate for small ensembles, ~ 1. Nevertheless, for larger ensemble of particles, it is possible to gain more entanglement. The time in which the first minimum of χ^2 occurs $(2\pi\sqrt{N})$ increases by increasing of N. In addition, the concurrence is considered for $N = 2$ and we have found good agreement between regular peaks of the entanglement measures.

In the intermediate-field regime, the quantum Fisher information and spin squeezing begin to differ. Compared to the weak-field regime, the corresponding minimums of χ^2 and ξ^2 decrease, while $\chi^2 < \xi^2$. Moreover, the minimums may occur in long-time scales.

When the field increases continuously, the fully different behavior of χ^2 and ξ^2 is observed. While for strong-field amplitude, it has already been studied that spin squeezing approaches unity [30], the quantum Fisher information predicts considerable entanglement. For $N = 2$, χ^2 regains a quasiregular pattern with period $\pi\sqrt{\bar{n}}$ and minima which coincide with concurrence peaks. Considering N number of particles, the time for the first minimum of entanglement is close to $\sim\pi\sqrt{\bar{n}}/N$. Thus, as opposed to the weak-field regime, by increasing N (and fixed $\bar{n}$), entanglement appears at shorter times, $\propto N^{-1}$. For very strong coherent fields, there is no multiparticle entanglement as expected.

VI. CONCLUSION

Aristotle once said "the whole is something beside the parts" [53]. The Dicke model is a very good physical manifestation of this perception. In this paper, we have provided a simple scheme for generating and detecting multiparticle entanglement. By changing the initial coherent field, we have evaluated the entanglement, making use of quantum Fisher information. In comparison to spin squeezing, we have found more entanglement in a wider range of initial field states. Due to the intrinsic connection of the Fisher information to estimation theory, the useful entanglement detected between particles can be exploited for atomic interferometric purposes. Specifically, in small ensemble of spins, the effectiveness of the QFI in a strong-field regime makes it a useful tool in detecting mesoscopic cat states of particles or collapse and revival of entanglement [51,52].

To conclude, we would like to comment on two different important points. First, in a many-body system with very large number of particles, measurement of the quantum Fisher information needs the full tomography of the atomic density matrix, which is a difficult task in practice. In this case, the measurement of Fisher information (as the lower bound of QFI) would be helpful in order to investigate the entanglement [27,29]. Without relying on tomographic reconstruction of the atomic quantum state, the method [27] utilizes a specific set of experimental probability distributions after small rotations of the quantum states. The Euclidean distance in the space of probability amplitudes—Hellinger distance—is related to Fisher information. Second, cavities are prone to atomic and photonic losses [54,55]. The realistic possibility to create entanglement depends on the competition

between the nonlinear unitary dynamics and decoherence, whose coupling parameters are determined by the specific experimental implementation.

ACKNOWLEDGMENTS

We kindly thank K. Mølmer, P. F. Buonsante, M. Gabbrielli, and L. Pezzé for useful discussions.

[1] R. H. Dicke, Phys. Rev. **93**, 99 (1954).
[2] M. Tavis and F. W. Cummings, Phys. Rev. **170**, 379 (1968).
[3] K. Baumann, C. Guerlin, F. Brennecke, and T. Esslinger, Nature (London) **464**, 1301 (2010).
[4] J. Klinder, H. Keßler, M. Wolke, L. Mathey, and A. Hemmerich, Proc. Natl. Acad. Sci. **112**, 3290 (2015).
[5] M. P. Baden, K. J. Arnold, A. L. Grimsmo, S. Parkins, and M. D. Barrett, Phys. Rev. Lett. **113**, 020408 (2014).
[6] K. Hepp and E. H. Lieb, Ann. Phys. NY **76**, 360 (1973).
[7] Y. K. Wang and F. T. Hioe, Phys. Rev. A **7**, 831 (1973).
[8] T. E. Tessier, I. H. Deutsch, A. Delgado, and I. Fuentes-Guridi, Phys. Rev. A **68**, 062316 (2003).
[9] A. Retzker, E. Solano, and B. Reznik, Phys. Rev. A **75**, 022312 (2007).
[10] H. T. Cui, K. Li, and X. X. Yi, Phys. Lett. A **365**, 44 (2007).
[11] J. A. Mlynek, A. A. Abdumalikov, Jr., J. M. Fink, L. Steffen, M. Baur, C. Lang, A. F. van Loo, and A. Wallraff, Phys. Rev. A **86**, 053838 (2012).
[12] F. Haas, J. Volz, R. Gehr, J. Reichel, and J. Esteve, Science **344**, 180 (2014).
[13] M. A. Nielsen and I. L. Chuang, *Quantum Computation and Quantum Information* (Cambridge University Press, Cambridge, 2000).
[14] V. Giovannetti, S. Lloyd, and L. Maccone, Science **306**, 1330 (2004)
[15] S. Hill and W. K. Wootters, Phys. Rev. Lett. **78**, 5022 (1997).
[16] D. J. Wineland, J. J. Bollinger, W. M. Itano, F. L. Moore, and D. J. Heinzen, Phys. Rev. A **46**, R6797(R) (1992).
[17] J. Appel, P. J. Windpassinger, D. Oblak, U. B. Hoff, N. Kjærgaard, and E. S. Polzik, Proc. Natl. Acad. Sci. USA **106**, 10960 (2009).
[18] I. D. Leroux, M. H. Schleier-Smith, and V. Vuletic, Phys. Rev. Lett. **104**, 073602 (2010).
[19] M. F. Riedel, P. Bohi, Y. Li, T. W. Hansch, A. Sinatra, and P. Treutlein, Nature (London) **464**, 1170 (2010).
[20] J. G. Bohnet, K. C. Cox, M. A. Norcia, J. M. Weiner, Z. Chen, and J. K. Thompson, Nat. Photon. **8**, 731 (2014).
[21] A. Sørensen, L. M. Duan, J. I. Cirac, and P. Zoller, Nature (London) **409**, 63 (2001).
[22] L. Pezze and A. Smerzi, Phys. Rev. Lett. **102**, 100401 (2009).
[23] P. Hyllus, O. Gühne, and A. Smerzi, Phys. Rev. A **82**, 012337 (2010).
[24] S. A. Diddams, J. C. Bergquist, S. R. Jefferts, C. W. Oates, Science **306**, 1318 (2004).
[25] S. D. Huver, C. F. Wildfeuer, and J. P. Dowling, Phys. Rev. A **78**, 063828 (2008).
[26] G. M. Tino and M. A. Kasevich, *Atom Interferometry, Proceedings of the International School of Physics Enrico Fermi, Course CLXXXVIII* (IOS Press, Amsterdam, 2014).
[27] B. Lücke, M. Scherer, J. Kruse, L. Pezze, F. Deuretzbacher, P. Hyllus, O. Topic, J. Peise, W. Ertmer, J. Arlt, L. Santos, A. Smerzi, and C. Klempt, Science **334**, 773 (2011).
[28] H. Strobel, W. Muessel, D. Linnemann, T. Zibold, D. B. Hume, L. Pezzé, A. Smerzi, and M. K. Oberthaler, Science **345**, 424 (2014).
[29] J. G. Bohnet, B. C. Sawyer, J. W. Britton, M. L. Wall, A. M. Rey, M. Foss-Feig, and J. J. Bollinger, Science **352**, 1297 (2016).
[30] C. Genes, P. R. Berman, and A. G. Rojo, Phys. Rev. A **68**, 043809 (2003).
[31] G. Vitagliano, P. Hyllus, I. L. Egusquiza, and G. Toth, Phys. Rev. Lett. **107**, 240502 (2011).
[32] B. Lücke, J. Peise, G. Vitagliano, J. Arlt, L. Santos, G. Tóth, and C. Klempt, Phys. Rev. Lett. **112**, 155304 (2014).
[33] A. S. Sørensen and K. Mølmer, Phys. Rev. Lett. **86**, 4431 (2001).
[34] C. Weiss and N. Teichmann, J. Phys. B **42**, 031001 (2009).
[35] F. T. Arecchi, E. Courtens, R. Gilmore, and H. Thomas, Phys. Rev. A **6**, 2211 (1972).
[36] This is done by using the covariance matrix given in Ref. [23].
[37] This can be done by use of the covariance matrix given in Ref. [40] or by making appropriate rotations in the normal plane [30].
[38] A. B. Klimov and S. M. Chumakov, *A Group-Theoretical Approach to Quantum Optics* (Wiley-VCH, Weinheim, 2009).
[39] M. Kozierowski, S. M. Chumakov, and A. A. Mamedov, J. Mod. Opt. **40**, 453 (1993).
[40] J. Ma, X. Wang, C. P. Sun, and F. Nori, Phys. Rep. **509**, 89 (2011).
[41] N. Lambert, C. Emary, and T. Brandes, Phys. Rev. A **71**, 053804 (2005).
[42] G. Ramon, C. Brif, and A. Mann, Phys. Rev. A **58**, 2506 (1998).
[43] Precisely, we have considered a discrete set of initial intensities within $\bar{n} \leqslant N$. One might consider also $\bar{n} \geqslant N$ in this regime, though the numerical simulations get more unwieldy by increasing both N and $\bar{n}$ and, for strong enough coherent fields, it is better to use the method in Sec. IV C.
[44] S. M. Chumakov, A. B. Klimov, and J. J. Sanchez-Mondragon, Phys. Rev. A **49**, 4972 (1994).
[45] J. C. Retamal, C. Saavedra, A. B. Klimov, and S. M. Chumakov, Phys. Rev. A **55**, 2413 (1997).
[46] Since Markoff approximation breaks in the limit of $t \ll \sqrt{\bar{n}}/g$, reduced density matrix (20) does not give the correct value at $t = 0$.

[47] S. Agarwal, S. M. Hashemi Rafsanjani, and J. H. Eberly, Phys. Rev. A **85**, 043815 (2012).
[48] B. Mollow, Phys. Rev. A **12**, 1919 (1975)
[49] Note that $\langle S_z \rangle = 0$, as we have used the Markoff approximation which is valid for shorter times than the collapse and revival of population inversion.
[50] Using Eq. (20), we get $\langle [S_\alpha, S_\beta]_+ \rangle = 0$ for $\alpha, \beta = x, z$. Therefore, the minimum value of spin squeezing (8) is either along x or z [40].
[51] C. E. A. Jarvis, D. A. Rodrigues, B. L. Gyorffy, T. P. Spiller, A. J. Short, and J. F. Annett, New J. Phys. **11**, 103047 (2009).
[52] S. Dooley, F. McCrossan, D. Harland, M. J. Everitt, and T. P. Spiller, Phys. Rev. A **87**, 052323 (2013).
[53] W. D. Ross, *Aristotle's Metaphysics* (Oxford University Press academic monograph reprints, 1924).
[54] H. P. Bauer and F. Petruccione, *The Theory of Open Quantum Systems* (Oxford University Press, Oxford, 2002).
[55] C. Hermann-Avigliano, N. Cisternas, M. Brune, J.-M. Raimond, and C. Saavedra, Phys. Rev. A **91**, 013815 (2015).